JMEPEG (2006) 15:149-154
DOI: 10.1361/105994906X95797

1059-9495/$19.00

# Liquid Impact of Chemical Vapor-Deposited Diamond-Coated Germanium and Zinc Sulfide Infrared Transmitting Materials

*M.J. Jackson, J.E. Field, E.J. Coad, and R.H. Telling*

*(Submitted November 4, 2005; in revised form December 19, 2005)*

**This article discusses the effect of applying diamond coatings on the response characteristics of certain infrared (IR) transmitting materials. The predicted response characteristics are compared with experimental data generated using controlled liquid jet impacts produced by the multiple impact jet apparatus. The predicted response of a selection of IR transmitting materials compare well with the experimental results. The results presented in this article illustrate the importance of the first stages of liquid impact on the integrity of the surface coating applied to zinc sulfide and germanium substrates.**

**Keywords:** brittle materials, diamond coatings, fracture, infrared transmitting materials, liquid impact

## 1. Theory of Liquid Impact

The impact of a water drop is divided into two regimes (Ref 1-3). The first is when the contact edge travels across the surface of the target at a velocity, $V_c$, that is greater than the shock-wave velocity propagating into the water drop. The water behind the shock front, as a result of impact, is compressed because there are no free surfaces through which the pressure can be released (Fig. 1). The shock-wave velocity into the water drop is reasonably well described, up to impact velocities of 1000 m/s using the following equation:

$$C = C_o + \mathrm{kV} \quad \text{(Eq 1)}$$

where $C_o$ is the acoustic velocity, $V$ is the impact velocity, and $k$ is approximately equal to 2 (Ref 4). Under the impact conditions considered here, the pressure exerted on the surface of a rigid target is known as the *water-hammer pressure*, $P_c$ (Ref 5), which is described by the equation:

$$P_c = \rho CV \quad \text{(Eq 2)}$$

where $\rho$ is the density of the water, 1000 kg/m$^3$. If the compressibility of the target is taken into consideration, then the pressure in this initial regimen is:

$$P_c = \frac{V\rho_1\rho_2 C_1 C_2}{\rho_1 C_1 + \rho_2 C_2} \quad \text{(Eq 3)}$$

This paper was presented at the fourth International Surface Engineering Congress and Exposition held August 1-3, 2005 in St. Paul, MN.

**M.J. Jackson,** Center for Advanced Manufacturing, College of Technology, Purdue University, West Lafayette, IN 47907; and **J.E. Field, E.J. Coad,** and **R.H. Telling,** Cavendish Laboratory, University of Cambridge, Madingley Road, Cambridge, CB3 0HE, U.K. Contact e-mail: jacksomj@purdue.edu.

where $\rho$ is the density and $C$ is the shock-wave velocity. The subscripts refer to the liquid and solid, respectively. The water-hammer pressure is not constant over the loaded region, which has high-pressure peaks, up to three times the contact pressure, at the edge of the contact zone at the point where the shock wave overtakes the contact edge. These peaks have been predicted theoretically by Heymann (Ref 4) and Lesser (Ref 5), and measured experimentally by Rochester et al. (Ref 6). However, these edge pressures are of very short duration (usually a few nanoseconds) and can be ignored.

When the shock envelope overtakes the contact edge, a free surface is generated that allows the compressed region to release (Fig. 1c and d). The release waves propagate into the water drop from the free surfaces, thus reducing the pressure that is approximately the incompressible Bernoulli pressure, $P_i$, which is:

$$P_i = \frac{\rho V^2}{2} \quad \text{(Eq 4)}$$

For the velocities considered in this study, the $P_i$ is very much lower than the water-hammer pressure, with the precise value depending on the velocity, because the ratio of pressures is given by $2C/V$. The radius over which high pressure acts can be calculated by examining the geometry of the impacting drop and considering the critical angle between the drop at the contact surface and the target. The radius of release, $r$, is the point at which the shock wave travels faster than the velocity at the edge of contact, $V_c$. The release radius is:

$$r = \frac{RV}{C} \quad \text{(Eq 5)}$$

where, $R$ is the radius of the impacting drop. For a 4 mm diameter water drop impacting at 300 m/s, the radius at which release occurs is approximately 300 $\mu$m. The time at which the release occurs can also be calculated using the geometry of the impacting drop. The time, after impact, $\tau$, at which release first commences is:

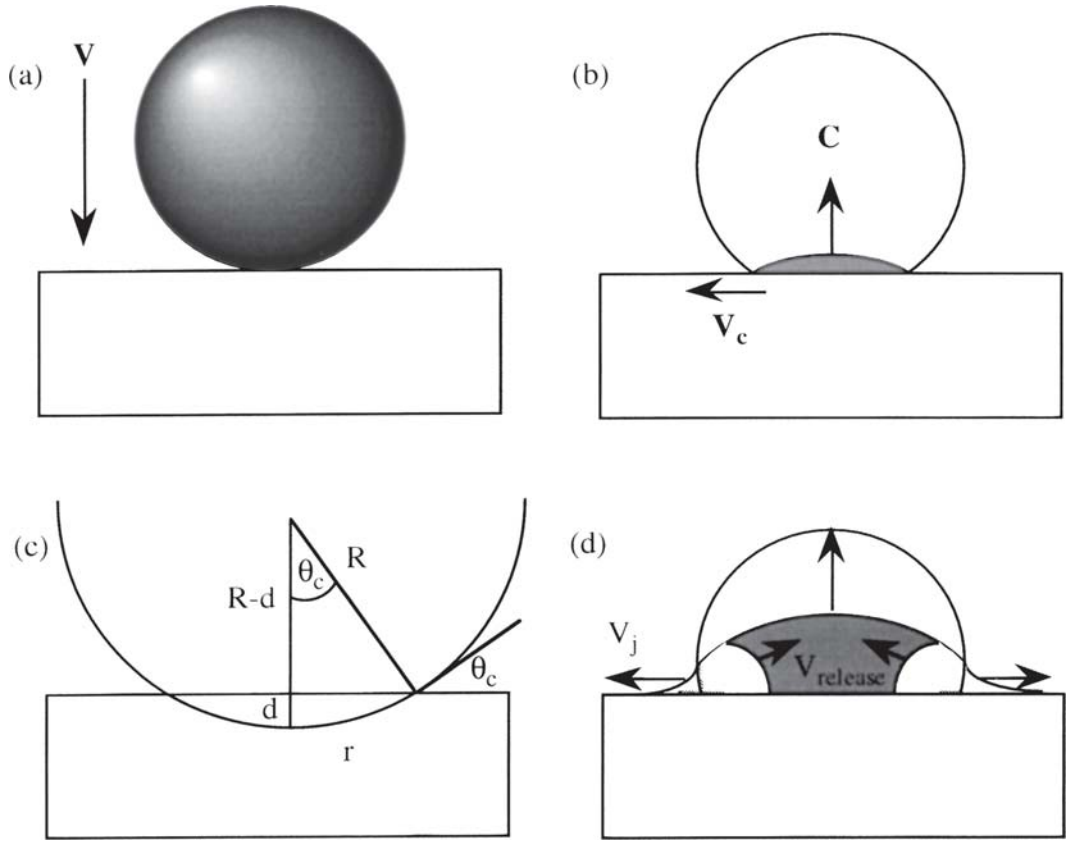


**Fig. 1** Sequence of liquid impact from the initial impact through to the release of high pressure (a) at impact, (b) where the water drop is compressed due to the lack of free surface, (c) at release, and (d) after the shock wave has overtaken the contact edge, allowing decompression and jetting. The dark regions in (b) and (d) represent the area of compressed fluid.

$$\tau = \frac{RV}{2C^2} \qquad \text{(Eq 6)}$$

The release waves then propagate toward the center of the compressed region. The total time for complete decompression is given by Lesser and Field (Ref 3):

$$\tau_{rel} = \frac{3RV}{2C^2} \qquad \text{(Eq 7)}$$

The duration of loading is very short. For example, the time for a 4 mm diameter drop to release is 0.2 μs for a 300 m/s impact. From Eq 5 and 7, it is clear that there are considerable changes in $r$ and $\tau$ with changes in the drop diameter $R$. There are various important implications from the theory of liquid impact. The first is that it is the initial stage of impact that generates the extreme pressures that lead to damage. The second is that the precise geometry in the contact region is critical in determining the duration of the high-pressure stage. For example, if the radius of curvature of a drop at contact with a plane surface is double that of a sphere of equivalent volume, then $\tau$ is similarly doubled. The circumferential crack pattern that is produced after impact is generated by the interaction of the Rayleigh surface wave with preexisting cracks in the surface of the material (Ref 2) (Fig. 2). Liquid impact is conveniently studied in the laboratory by extruding a stream of water of known volume through a nozzle or jet. It is possible to relate the damage caused by a particular size of jet to that produced by an "equivalent" spherical drop (Ref 7). The point at which circumferential damage becomes visible at a particular velocity is known as the *damage threshold velocity* (DTV).

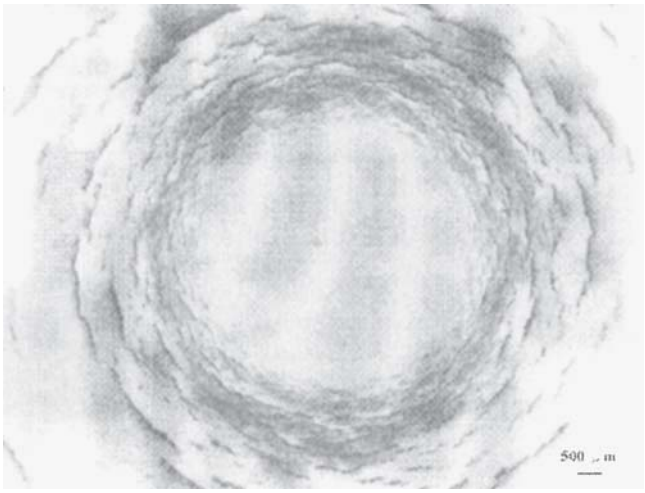

**Fig. 2** Liquid impact damage on zinc sulfide showing a series of circumferential fractures caused by the Rayleigh wave interacting with preexisting surface cracks. The impact velocity was 300 m/s.

The dynamic criterion for crack growth and, thus, strength loss is given by Steverding and Lehnigk (Ref 8) as:

$$\sigma^2\tau = const \qquad \text{(Eq 8)}$$

For liquid impact by water drops, Eq 8 becomes:

$$\sigma^2\tau = \frac{3\rho^2}{2} RV^3 \quad \text{(Eq 9)}$$

where $\sigma$ is the impact, or water-hammer, pressure and $\tau$ is the release time (refer to Eq 7) (Ref 8). This equation can be used to predict the DTV for different sizes of water drops, $R_1$ and $R_2$, if the DTV for one of the drop sizes is known. As $\sigma^2\tau$ is constant between the two drops, Eq 9 can be used to find the water-drop radius ratio:

$$\frac{R_1}{R_2} = \left(\frac{V_2}{V_1}\right)^3 \quad \text{(Eq 10)}$$

where $V_1$, is the DTV for crack extension for a water drop of radius, $R_1$. If a water drop is distorted in such a way that it has a profile equivalent to an effective increase in the radius of a factor of two, then the threshold velocity, $V_2$, is equal to $2^{-1/3}$ $V_1$. There are three stress waves associated with the target when impacted. There are two bulk waves (compression and shear) that propagate outward into the target from the impact point attenuated in proportion to $r^{-2}$ on the surface, and $r^{-1}$ in the bulk of the target material, respectively. The compression wave is the fastest, with a velocity $C_1$. A second slower wave is the shear wave with velocity, $C_2$, approximately two thirds of $C_1$, with the exact ratio dependent on the Poisson's ratio of the target material. Note that with an anisotropic material there will be two shear waves. The compression wave has little effect on the damage pattern. However, when it reflects and changes phase to a tensile wave, it can cause fracture. This is particularly important with small specimens. With thin plates, reflected waves from the rear surface can reinforce the front surface Rayleigh wave and cause bands of fracture. The analysis can be found in Field (Ref 1) and Bowden et al. (Ref 2). The third wave is the Rayleigh surface wave, which interacts with surface cracks. The velocity of the Rayleigh wave is approximately equal to 0.6 $C_1$. The wave is confined to the surface and attenuates at a lower rate, proportional to $r^{-1/2}$, compared with surface bulk waves. The Rayleigh wave has both vertical and horizontal components, and the depth to which the Rayleigh wave penetrates depends on the wavelength, which in turn depends on the impact velocity and the drop radius. The energy of the impact favors the Rayleigh surface wave with 67.4% of the total energy of the impact, the shear wave with 25.8% of the total energy, and the compression wave with 6.9% of the total energy (Ref 9, 10). Field (Ref 1) and Bowden et al. (Ref 2) discuss the role of the Rayleigh wave in producing circumferential cracks around the impact site.

## 2. Liquid Impact of Brittle Materials

### 2.1 Circumferential Damage

The typical damage pattern induced on the surface of a brittle material shows an undamaged region in the center and a clearly defined point, the release radius, at which damage is initiated (Fig. 2). This can be explained by considering the decelerating contact edge. When the contact velocity drops below that of the Rayleigh wave, the surface wave emerges and interacts with surface cracks. The cracks are distorted and tend to have a raised lip away from the impact center (Ref 7). As the Rayleigh wave moves away from the center of impact, it is dispersed by interaction with surface cracks and distorts to a broader, less intense, pulse. The very sharp intense wave at the release radius extends many surface cracks by a short distance. As the wave propagates, the width of the wave increases and the magnitude tends to decrease due to attenuation and interaction with cracks. The result is, at a greater radius, only the longer cracks are extended due to the greater stress intensity at the tip of the crack. At the edge of the visible damage, the wave has become so dispersed that it can only extend very large cracks, larger than are intrinsically seen in the material. When polishing scratches are present on the surface, they may be sufficiently large enough to extend. With single-crystal materials and high-temperature high-pressure diamond, the damage pattern consists of the opening of cleavage planes, and in the case of chemical vapor-deposited (CVD) diamond, the damage consists of reinforced ring cracks.

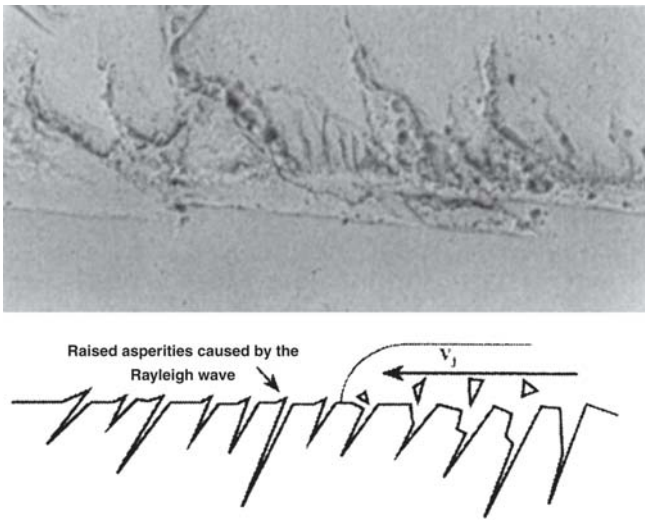


**Fig. 3** The damaging effects of lateral jetting. The left-hand side of the image shows damage by the Rayleigh wave only. As lateral jetting crosses the surface, it tears any asperity it collides with.

### 2.2 Lateral Jetting

When the shock wave moves to the free surface of the water drop and release commences, the water drop begins to spread across the surface of the material. The interaction of the water droplet with the target causes a high-velocity sideways jet of fluid (Ref 11) that has a velocity, $V_j$, that is faster than the impact velocity $V$. Lateral jetting exploits surface asperities that arise from surface roughness or damage, introduced by the Rayleigh surface wave, resulting in material loss and the further extension of cracks (Fig. 3). Jackson et al. (Ref 12) have discussed the contribution of lateral jetting to material loss in single-crystal materials.

### 2.3 Central Damage

In some materials, liquid impacts produce local failure on, or near, the impact axis. Bowden et al. (Ref 7) discovered this effect with polymethylmethacrylate (PMMA). In this particular case, the damage was located below the surface at a depth of about half the contact radius $r$. This is where Hertz's theory of elastic contact would predict the maximum shear

stress, as explained by Bowden et al. (Ref 7). However, for stress-dominated loading this is unlikely to be the full explanation. Recent experiments reported by Obara et al. (Ref 13) have shown that subsurface axial cracks in PMMA form when release waves from the contact periphery interact with bulk waves. Interestingly, release waves travel into the liquid-causing cavitation where they overlap. This has been discussed by Field et al. (Ref 11) and has been shown experimentally by Brunton and Camus (Ref 14). When cavities eventually collapse, they could damage the surface. A third damage mechanism is related to compressive or shear loading, which generates tensile failure at the boundaries between grains depending on their orientation or anisotropy. Once a pit develops, hydraulic loading could develop damage, as shown by Field (Ref 15). Obara et al. (Ref 13) used a larger diameter jet, which at 600 m/s would simulate water drops with a diameter in the region of 8 mm. These experiments, which involved high-speed framing and streak photography, allowed four damage modes to be identified: front surface Rayleigh wave damage (the dominant mechanism); subsurface, on-axis failure; spalling adjacent to the rear surface; and internal damage due to stress wave reinforcement. In the rain erosion situation where most of the drops have an average diameter of 2 to 3 mm (Ref 16), Rayleigh wave damage (circumferential damage) is the dominant mechanism leading to strength loss and damage. Experimental DTV curves use observations of circumferential damage as the mode of failure in brittle materials subjected to liquid impact.

### 2.4 Single Liquid Impact Apparatus

There have been a large number of rain erosion and liquid impact devices developed over the past 75 years. One of the earliest inventions, using repeated liquid impacts, was the wheel and jet. The device consisted of a continuous jet of water that was interrupted by a rotating wheel. The sample was mounted on the wheel, such that the impact velocity was the relative velocity between the sample and the water jet. Because the impact duration was quite short, the velocity of the jet was ignored. The maximum velocity of the waterjet was 250 m/s (Ref 15). This design was improved and redesigned over the following 20 years until a maximum velocity of 600 m/s was achieved. The erosion of blades in steam turbines stimulated this early work. This again is a situation where high-velocity water drops (300 m/s) impact high-strength alloys. However, the lifetime of a turbine blade ideally ends a few years before the erosion of the blade tip affects turbine efficiency. Other more elaborate rain erosion devices simulate flight through a rainfield. The whirling arm rig consists of a blade that rotates at high velocity with the test sample located at the end of an arm. The rig has a series of nozzles that generate a field of water droplets that impact the rotating sample. The advantage with this apparatus is that a simulated rainfield is produced, and long periods of exposure to intense rainfields are possible. However, the disadvantage of using the apparatus is that the exact shape of the impacting water drops is not known. There is also a risk of dust contamination during operation that results in an erosive environment. Another test method is the use of a rocket sledge passing through a series of artificial rainfields equally spaced along a test track. The sample is attached to the front of the rocket, which is fired with a peak velocity of 500 m/s. The advantage of using this method is that it simulates almost all of the effects of flight through a rainfield (such as factors affected by the aerodynamics of the shape of the dome). However, the cost of the testing is approximately $100,000 per specimen.

The final and most realistic test is to attach the test specimen onto the front of a missile, or aeroplane. Multiple liquid impact testing started with the use of the wheel-and-jet apparatus. The maximum velocity obtained was initially 150 m/s, but this was increased to 250 m/s and was used mainly for long periods of erosion. The use of liquid jets for damage studies started with a single-jet apparatus that was developed by Brunton (Ref 14). This apparatus used a spring-loaded air gun to fire a 0.22 caliber slug into the rear of a water-filled chamber that was sealed with a neoprene diaphragm. A high-speed coherent jet emerges from a nozzle if the dimensions of the chamber are designed correctly. The jet velocity was approximately five times the slug velocity (i.e., velocities of up to 1000 m/s could be achieved). Field (Ref 1) showed that velocities of several thousand meters per second could be reached by replacing the air gun with a rifle. Subsequently, Field et al. (Ref 9) improved the single-impact apparatus by using high-pressure gas and a fast-acting solenoid valve to fire the gun. A whole range of chambers was designed with diameters ranging from 0.4 to 3.2 mm. The jets were coherent and, after a distance of 10 mm through the air, were ablated such that their front profiles were smooth and curved. In the 1970s, the experimental production of jets and the development of the theory produced advances that would enable drop damage to be simulated by jet impact. The latest version of the single-impact jet apparatus (SIJA) has a velocity measurement device connected to it. The complete system is known as the SIJA. The SIJA can be used in conjunction with a hydraulic bursting disc apparatus that allows residual strength measurements to be made to disc specimens. By impacting a material at steadily increasing speeds and measuring the residual fracture strength, postimpact, a threshold velocity (i.e., the velocity at which the fracture strength drops due to the crack extension from the impact) can be obtained. The advantages of using the SIJA imply that high velocities can be achieved, a reasonable shot rate (15 $h^{-1}$) can be achieved, the repeatability of the velocity measurements is very high (5% spread), and the cost per shot is low (approx.imately $5 per shot). The disadvantage of using the SIJA is that a large number of samples are needed to generate a residual strength curve, and, due to the time between impacts, erosion studies are not possible.

### 2.5 Multiple Impact Jet Apparatus

The multiple-impact jet apparatus (MIJA) is a modified version of the SIJA. The development of an MIJA began in 1984, and it uses the same firing chamber design. However, a high-velocity piston replaces the projectile. Field (Ref 1) realized that if the apparatus is mounted vertically, no diaphragm would be needed to keep the water from flowing from the rear of the chamber, with surface tension preventing the liquid from escaping through the nozzle. Davies used this configuration to develop the first MIJA (Ref 9). Seward (Ref 17) described the further development of the MIJA, and a schematic diagram of the device is shown in Fig. 4. The firing sequence takes approximately 5 s. The auxiliary pressure vessel is maintained at a pressure that is slightly higher than that of the main pressure vessel. The pressure difference forces a plunger in a downward motion, sealing off the main body of the apparatus from the main pressure vessel. The firing mechanism merely involves evacuating the auxiliary pressure vessel (owing to the small

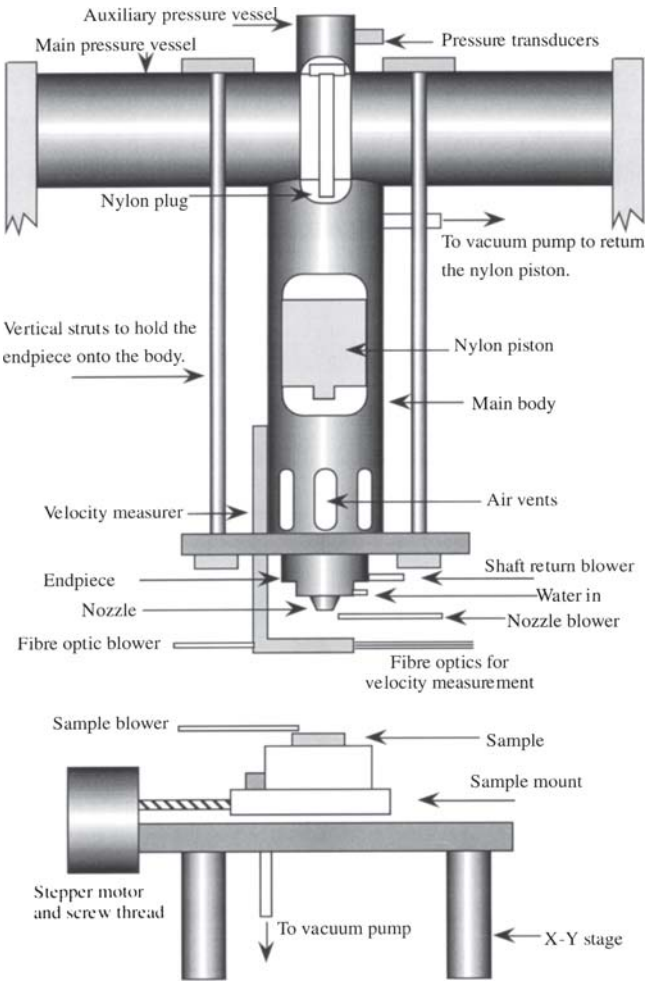


**Fig. 4** Absolute DTV (after 300 impacts) as a function of the logarithm of the static fracture toughness for a number of brittle materials. Water drop diameter, 2 mm

volume of the chamber). This produces a pressure difference across the plunger, forcing it in an upward direction. The compressed air in the main vessel then passes into the main body of the apparatus, forcing the nylon piston to impact against the raised shaft. The shaft stands proud of the nozzle on a cushion of air. There are vents at the base of the main body that allow air to flow out so that there is no cushioning effect on the piston. The titanium shaft is accurately guided into the nozzle by a linear bearing. The jet is produced as the water is forced through an 0.8 mm diameter orifice. After the water jet has impacted the sample under examination, three air blowers clear the nozzle, the target surface, and the fiberoptic links. The nylon piston is returned to the top of the main body by a vacuum pump, and the shaft is returned to its original position by the cushion of air. The nozzle is then refilled with water by means of a peristaltic pump. The firing process is controlled entirely by a computer.

The maximum jet velocity obtained for the MIJA is 650 m/s with a velocity spread of approximately 0.5 to 1% (considerably better than that for the SIJA). Owing to the high shot rate (up to 12 $min^{-1}$), and the resolution of the *X-Y* stage, accurate damage threshold curves and random arrays are possible. Additionally, a full damage threshold curve can be obtained from a 25 mm diameter sample. The facility to conduct erosion studies has allowed comparison with the whirling arm system

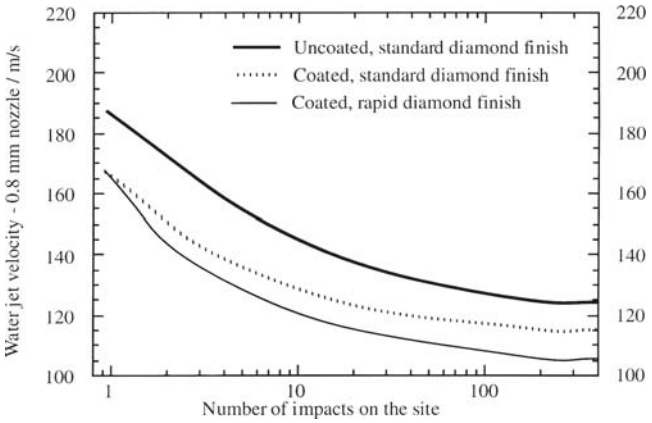


**Fig. 5** Damage threshold curves for coated and uncoated ZnS with a machined finish

that has been the main liquid erosion apparatus used for these tests. The difference between the two rigs is that the MIJA allows repeatable jet sizes (corresponding to equivalent drop sizes) to be impacted rather than a spread in drop sizes as demonstrated when using the whirling arm apparatus.

### 2.6 Experimental Results and Discussion

Experimental evidence of a material having a defined damage threshold curve is possible using an apparatus that has the characteristics of the MIJA. The accurate control of impact position, impact rate, and impact velocity means that a sample of material measuring approximately 20 mm in diameter can be used to generate a damage threshold curve. Up to 20 impact sites are designated within the boundary of the specimen, each with a different velocity assigned to it. These sites must be at least 5 mm apart from the edge, so those cracks from different sites do not interact with each other. Each site is impacted once at its assigned velocity. The specimen is examined using an optical microscope at magnifications of 40 and 100× to inspect the occurrence of circumferential impact damage. Impact sites that remain undamaged are subjected to further impacts and are reexamined using the optical microscope. The impact process is repeated until each site has been impacted 300 times. The characteristic damage threshold curve is a function of the number of impacts occurring at particular velocities. The damage threshold point at 300 impacts is assumed to be the absolute DTV of the target material. At velocities below this point, circumferential damage is not developed. This is because the energy provided by liquid impact is not significant enough to extend cracks up to the visible limit. The target materials used in this investigation were ZnS, Ge, diamond-coated ZnS, and diamond-coated Ge. All materials were polycrystalline. Figure 5 shows the damage threshold curve for an uncoated and coated ZnS substrate with an initially diamond-machined surface.

Figure 6 shows the damage threshold curve for an uncoated substrate and a coated ZnS substrate with a polished surface. Table 1 shows the improvements offered by using CVD diamond coatings on a number of different substrates.

Table 1 shows the effect of coating substrates on the DTV of a number of infrared (IR) substrates. The mechanism of protection appears to be enhanced by matching the acoustic properties of the substrates to the coatings.

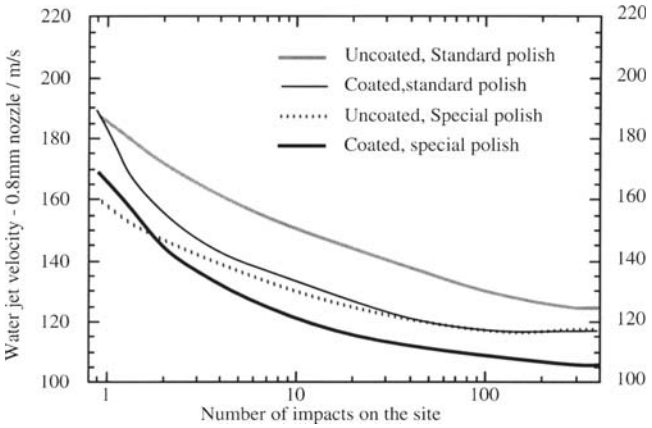


**Fig. 6** Damage threshold curves for coated and uncoated ZnS with a polished finish

**Table 1 Improvements offered by using CVD diamond coatings on a number of different substrates**

| Substrate material | Samples tested, No. | Uncoated damage threshold velocity, $ms^{-1}$ | Optimum coated damage threshold velocity, $ms^{-1}$ |
|---|---|---|---|
| Silicon | 7 | 210 ± 10 | 325 ± 25 |
| Germanium | 12 | 130 ± 5 | 313 ± 12 |
| Zinc sulphide | 2 | 125 ± 5 | 213 ± 12 |
| Sapphire | 1 | 425 ± 25 | 565 ± 15 |

## 3. Conclusions

It has been shown that the MIJA can be used to simulate water-drop impact conditions on a number of IR-transmitting materials. The CVD diamond coatings offer significant protection to substrates that are highly polished.

### References


1. J.E. Field, "The Deformation and Fracture of Brittle Solids," Ph.D. dissertation, Cavendish Laboratory, University of Cambridge, 1962
2. F.P. Bowden and J.E. Field, The Deformation of Solids by Liquid Impact, Solid Impact and by Shock, *Proc. R. Soc. London,* 1964, **A282,** p 331-352
3. M.B. Lesser and J.E. Field, The Impact of Compressible Liquids, *Ann. Rev. Fluid Mech.,* 1983, **15,** p 97-122
4. F.J. Heymann, High Speed Impact Between a Liquid Drop and a Solid Surface, *J. Appl. Phys.,* 1969, **40,** p 5113-5122
5. M.B. Lesser, Analytic solutions of liquid drop impact problems, *Proc. R. Soc. London,* 1981, **A377,** p 289-308
6. M.C. Rochester and J. Brunton, ″H: Pressure Distributions During Drop Impact," Paper 6, Proc. 5th Int. Conf. "Erosion by Liquid and Solid Impact," Cavendish Laboratory, University of Cambridge, Cambridge, U.K., 1979
7. F.P. Bowden and J.H. Brunton, The Deformation of Solids by Liquid Impact at Supersonic Speeds, *Proc. R.. Soc. London,* 1961, **A263,** p 433-450
8. B. Steverding and S.H. Lehnigk, Dynamic Thresholds for Crack Propagation, *Int. J. Fract. Mech.,* 1969, **5,** p 369-370
9. J.E. Field, D.A. Gorham, J.T. Hagan, M.J. Matthewson, S.V. Swain, and S. van der Zwaag, "Liquid Jet Impact and Damage Assessment for Brittle Solids," Paper 13, Proc. 5th Int. Conf. "Erosion by Liquid and Solid Impact," Cavendish Laboratory, University of Cambridge, Cambridge, U.K., 1979
10. G.F. Miller and H. Pursey, On the Partition of Energy Between Elastic Waves in a Semi-Infinite Solid, *Proc. R.. Soc. London,* 1956, **A233,** p 55-69
11. J.E. Field, M.B. Lesser, and J.P. Dear, Studies of Two-Dimensional Liquid Wedge Impact and the Relevance to Liquid-Drop Impact Problems, *Proc. R. Soc. London,* 1985, **A401,** p 225-249
12. M.J. Jackson and J.E. Field, Liquid Impact Erosion of Single Crystal Magnesium Oxide*, Wear,* 1999, **233-235,** p 39-50
13. T. Obara, N.K. Bourne, and J.E. Field, Liquid Jet Impact on Liquid and Solid Surfaces, *Wear,* 1995, **186-187,** p 338-344
14. J.H. Brunton and J.-J. Camus, "The Application of High-Speed Photography to the Analysis of Flow in Cavitation and Drop Impact Studies," presented at Proc. 9th Int. Congress "High Speed Photography" (Denver, CO), 1970
15. J.E. Field, "The Importance of Surface Topology on Erosion Damage," presented at 2nd Int. Conf. "Rain Erosion & Assoc. Phenom.," Royal Aircraft Establishment (Farnborough, U.K.), 1967, p 593-603
16. J. Denis and D. Balageas, "Rain Erosion Resistance of Infra-Red Materials," Paper 19, presented at Proc. 5th Int. Conf. "Erosion by Liquid and Solid Impact," Cavendish Laboratory, University of Cambridge, U.K., 1979
17. C.R. Seward, "Rain Erosion Testing of Infra-Red Window Materials," Ph.D. dissertation, Cavendish Laboratory, University of Cambridge, 1992